

Electron Backscattering Assists Solid Harmonic Generation From Bilayer Infrastructure

Chao Yu,¹ Shicheng Jiang,¹ Tong Wu,¹ Guanglu Yuan,¹ Yigeng Peng,¹ Cheng Jin,¹ and
Ruifeng Lu^{1,2,*}

¹*Department of Applied Physics, Nanjing University of Science and Technology, Nanjing
210094, P R China*

²*State Key Laboratory of Molecular Reaction Dynamics, Dalian Institute of Chemical
Physics, Chinese Academy of Sciences, Dalian 116023, P R China*

In the framework of time-dependent density functional theory, we find a much extended high-order harmonic generation from bilayer crystals with large interlayer spacing of several nanometers. An ultrafast strong laser with grazing incidence to such kind of infrastructures leads to a clear double-plateau structure in harmonic spectrum. Traditional three-step model fails in interpreting the second plateau of photon energy far beyond atomic-like harmonics. Here, we propose a four-step model which includes the backscattering of the ionized electrons to understand the cutoff extension, and our classical model well explains this backscattering process. Moreover, the cutoff is continuously extended with increasing the interlayer spacing of planar crystals and the conversion efficiency in the second plateau is significantly enhanced by driving laser with longer wavelengths. This work thus establishes a novel and efficient way to produce high-energy light source up to soft X-ray region at nanoscale, which could be utilized as a compact platform for attosecond photonics.

* rflu@njjust.edu.cn

As one of the most prominent methods to develop attosecond science, high-order harmonic generation (HHG) from gaseous media has been studied extensively over several decades [1–5]. Two main challenges for further HHG experiments are well known: (i) continuously increasing the harmonic conversion efficiency and (ii) extending the cutoff energy to achieve practical attosecond photonics [6]. Recently, the possibility of realizing efficient high harmonics from solid materials has attracted much attention [7–17], which offers opportunities to obtain extreme ultraviolet sources [11, 18–20] and study ultrafast electron dynamics in condensed matters [21, 22].

Remarkably, Luu et al. [11] applied a sub-cycle synthesized field with bandwidths that covers the ultraviolet and near-infrared spectral regions to a silicon dioxide crystal and showed the total photon yield of fused silica is higher than the noble gases. In search of more efficient solid media for HHG, two-dimensional (2D) materials have become the focus of research, such as graphene [13, 23–25], monolayer molybdenum disulphide (MoS_2) [13, 26] and hexagonal boron nitride (h-BN) [27–29]. In this regard, Yoshikawa et al. [13] observed the HHG signal in graphene dramatically enhanced under elliptically polarized excitation. Compared to the MoS_2 bulk, Liu et al. [26] found the harmonic efficiency per layer exhibits significant enhancement in layered structures. Besides, Tancogne-Dejean et al. [27] predicted that monolayer and few-layer materials are promising for efficient HHG because of their strong inhomogeneity of the electron-nuclei potential.

In solid HHG, the energy cutoff scales linearly to the peak field [7] and it also depends strongly on the electronic band structure [11, 30]. However, the maximum intensity that could be applied to a bulk material is intrinsically limited by its damage threshold. Hence, the cutoff of solid HHG is in principle restricted by the peak intensity of driving laser and maximum energy gap at the Brillouin zone edge [31, 32]. Unfortunately, the existing experiments also indicate that the cutoff in solid harmonic spectrum is unfavorable compared to that from gases which can reach the soft X-ray range [16]. More recently, Tancogne-Dejean et al. [33] demonstrated atomic-like HHG in monolayer h-BN when laser polarization is perpendicular to the material surface. Indeed, this is an interestingly novel approach for generating high-order harmonics based on a solid-state device, with an energy cutoff and a more favorable wavelength scaling of the harmonic yield similar to those in atomic and molecular gases.

Since the atomic-like HHG in monolayer takes both advantages of high cutoff energy in gases and high conversion efficiency in solids [33], we extend the 2D target to bilayer geometry to explore the interlayer effect in solid HHG. In this letter, we take h-BN as the prototypical case. The bilayer h-BN infrastructure is constructed with large interlayer spacing at the order of nanometers. We are not aiming at discussion of interlayer coupling inside the bilayer with equilibrium distance less than 4 angstrom, which has been already addressed to some extent [34]. In fact, the stacking pattern and ingredient of distant bilayer will not affect the main conclusions. Also, more complicated infrastructure analogous to metasurface [35] is not the scope of this work. To drive the ionization of electron populated on the valence band of h-BN without

damage, we use a strong laser grazing incidence to the material surface. In the framework of time-dependent density functional theory (TDDFT), the HHG spectra of monolayer h-BN and distant bilayer h-BN were simulated by the state-of-the-art Octopus code [36]. It is very encouraging that this ab initio code has successfully studied the ellipticity-dependence HHG in bulk silicon and MgO [37], the polarization-state-resolved high-harmonic spectroscopy from silicon [38], and HHG in some complex systems, such as strongly correlated material [39] and spin-polarised h-BN with defects [40]. We included a full description of electron-electron and electron-ion interactions in TDDFT calculations, and more numerical details are provided in supplemental materials.

In Fig. 1, the simulated high harmonic spectra from monolayer, bilayer h-BN with interlayer spacing of $d = 40$ angstrom (4 nm) and $d = 70$ angstrom (7 nm) are displayed. We choose almost the same laser parameters in Ref. 33. The laser polarization is perpendicular to the h-BN surface and the peak intensity is $I = 1.0 \times 10^{14}$ W/cm². The laser wavelength is 1600 nm and the full width at half maximum of the Gaussian-envelop laser is 15 fs. The calculated work function E_w of monolayer h-BN is about 6.0 eV within the adiabatic local density approximation, suggesting that layered h-BN can be exposed to such intense and short laser for an out-of-plane electric field without damage [33]. In addition, under such laser parameters, Zener

tunneling dominates the transition according to Keldysh parameter $\gamma = \sqrt{\frac{E_w}{2U_p}}$, where

$U_p = I/4\omega^2$ is the ponderomotive energy of the electron in the applied laser field. For monolayer h-BN, the emitted harmonics present atomic-like HHG features [33] and the cutoff energy shown in Fig. 1 (green line) is in very good agreement with the predicted value ($E_{\text{cutoff}} = E_w + 3.17 U_p$) by the three-step model [41, 42]. Fig. 2(a) schematically plots the physical processes in traditional three-step model for HHG from monolayer h-BN. First, electrons are released via tunneling near each peak of electric field. In a periodically oscillating laser field, the electrons will be driven to the farthest point where their velocity becomes zero during about half optical cycle. Then, electrons could be accelerated by the laser field in reverse direction and return back to monolayer h-BN. Finally, they recombine with the parental material, releasing the energy acquired by acceleration in the form of photon emission.

Quite different from the monolayer case, the harmonic spectra of bilayer h-BN with large interlayer spacing present a distinct double-plateau profile, as shown in Fig. 1 with blue line for $d = 40$ angstrom and red line for $d = 70$ angstrom. Apparently, the cutoff energy values corresponding to the first plateaus for both $d = 40$ angstrom and $d = 70$ angstrom are almost the same as that of the monolayer, which indicates that the atomic-like three-step model in Fig. 2(a) also dominates the harmonic emission in the first plateau. However, the second plateau with photon energy far beyond the atomic-like HHG could not be interpreted by three-step model. Ab initio simulation results show that the cutoff values of the second plateaus are tremendously extended to $E_w + 4.89 U_p$ and $E_w + 9.53 U_p$ for $d = 40$ angstrom and $d = 70$ angstrom, respectively.

To understand these extraordinary extension regarding the second plateau, we

propose a four-step model shown in Fig. 2(b): (i) electrons are released from each h-BN monolayer, (ii) as the electronic movement is confined by interlayer space, the electrons will be backscattered when they are driven from one layer to the other, (iii) electrons are accelerated by the laser field in reverse direction and return back with a nonzero initial velocity after backscattering, (iv) electrons recombine with the parental layer releasing photons of higher energy. Please keep in mind that the first and the final steps (i.e. electrons releasing and recombining) in our four-step model are the same as those in traditional three-step model. Normally, a maximum energy of $10 U_p$ for harmonic emission can be achieved when electrons are scattered by 180° [43]. Therefore, the additional backscattering step that endows electron with a large initial velocity for the following acceleration is the key to form the second high-energy plateau.

For a more intuitive description of backscattering process, the time evolution of the induced electronic density for distant bilayer h-BN is shown in Fig. 2(c). The interlayer spacing here is $d = 40$ angstrom and laser parameters are the same as those in Fig. 1. Clearly, the time-dependent electronic wavepackets evolve in bundles with two types of visible trajectories. These two types of trajectories that return to the parental layer both result in HHG. In more detail, the trajectories labeled by purple hollow arrows outside the bilayer represent the processes in traditional three-step model. Moreover, the brand-new trajectories between the two layers in four-step process are marked by white hollow arrows. As predicted, both types of trajectories are emerged periodically per half optical cycle, which means that trajectories either in three-step model or in four-step model lead to harmonic emission in every half optical cycle.

In order to study the harmonic spectra in time domain, time-frequency analyses of HHG from bilayer h-BN with $d = 40$ angstrom and $d = 70$ angstrom are presented in Fig. 3(a) and 3(b), respectively. As seen from Fig. 3(a), it can be determined that the harmonic spectra in time domain are comprised of two plateaus, one is originated from the three-step model with maximum energy of about $E_w + 3.17 U_p$ and the other is due to the four-step processes including backscattering with a cutoff reaching to $E_w + 4.89 U_p$. Within multiple optical cycles, several central peaks in the time-frequency maps corresponding to the second plateau are labeled as $P_1, P_2, P_3,$ and P_4 for convenience. Similar to the harmonic emission features in the first plateau, harmonics also burst in every half optical cycle in the second plateau, but the emission time of each peak in the second plateau is shifted earlier than that of the first plateau, which can be explained by the motion constraint of ionized electron inside the interlayer region.

For better elucidating the striking phenomena derived from TDDFT quantum calculations, we develop a simplified model based on classical Newtonian equation. In this classical model, the electronic motion in the aforementioned laser field $E_L(t)$ is described by $\ddot{x} = -E_L(t)$. Here, the Coulomb attraction to the parent layer is neglected and we assume the electron emerges on the outside of tunneling barrier with zero velocity $v(t_0) = 0$. Thus, the electron's velocity following the laser field can be

described by $v(t) = A_L(t) - A_L(t_0)$, where the vector potential $A_L(t)$ is defined by $E_L(t) = -A_L(t)/dt$. Backscattering takes place once the electrons arrive to the other layer. We note the type of backscattering calculated here is treated as an elastic scattering, which implies that the momentum of electron is reversed as $v_b(t) = -v(t)$ during backscattering. The classical ionization and recollision energy diagrams for bilayer h-BN with $d = 40$ angstrom and $d = 70$ angstrom are shown in Fig. 3(c) and 3(d), respectively. In Fig. 3(c), we clearly see that both long and short trajectories contribute to HHG in the first plateau, in consistent with the time-frequency analyses in Fig. 3(a). It is well established that a free electron can gain a maximum energy of $3.17 U_p$, and this limit obeys the cutoff position determined in the first plateau. Furthermore, the origin of the second plateau in HHG from bilayer h-BN with large interlayer spacing can be analyzed perfectly by our classical model which exactly computes the energy value of $4.89 U_p$ by a momentum reversion after backscattering. As well, three trajectories in Fig. 3(c) contribute to HHG in the second plateau, agreeing well with the time-frequency analysis in Fig. 3(a). Due to the trajectories (T_r **1** and T_r **2**) will be degenerated when the interlayer spacing is increased (see Fig. s1), we define the maximum energy of trajectory **3** (T_r **3**) as the cutoff energy. Compared to $d = 40$ angstrom, the electron can achieve an energy as high as $9.53 U_p$ in the second plateau for $d = 70$ angstrom (Fig. 3(d)).

Furthermore, the dependence of HHG on interlayer distance is provided in Fig. 4(a). The laser parameters are identical to those in Fig. 1. It is natural that the cutoff energy ($E_{\text{cutoff}} = E_w + 3.17 U_p$) of the first plateau is unchanged. For the second plateau, the purple line in Fig. 4(a) represents the cutoff values calculated by the classical model. The cutoff of the second plateau is extended near linearly with the increasing of the interlayer spacing of bilayer h-BN. However, the conversion efficiency of the second plateau is greatly weakened for larger interlayer spacing, which is understandable considering that the chosen laser condition allow less electrons to reach the other layer for $d > 70$ angstrom. In terms of the wavelength dependence, we simulated the HHG from distant bilayer with interlayer spacing fixed at $d = 70$ angstrom. In Fig. 4(b), the harmonic yield in the first plateau decreases drastically as the laser wavelength increased, because of a time-space spreading of the electron wave packet during its free evolution in vacuum [44, 45]. In bilayer infrastructure, the decrease in harmonic yield with increasing the interlayer spacing (Fig. 4(a)) can be attributed to the restricted spreading of the electron wave packet between the two layers. Nevertheless, increasing wavelength will permit slow electrons moving further in space, accordingly more electrons can travel from one layer to the other and are backscattered. As shown in classical ionization and recollision plots in Fig. s2, trajectories **1** and **2** are gradually survived. Therefore, the conversion efficiency of the second plateau is significantly enhanced with increasing the wavelength.

In conclusion, from ab initio TDDFT calculations together with quantum time-frequency and classical model analyses, we suggest a not yet discovered strategy to achieve high-intensity and high-energy harmonics from solids, i.e., with the merits

of electronic releasing and backscattering inside the bilayer crystals of interlayer spacing at the nanometer scale, a strong laser grazing incidence to the materials is anticipated to produce the second plateau with photon energy far beyond $E_w+3.17 U_p$, and the harmonic yield is hopefully enhanced by adjusting the interlayer spacing and wavelength. Distinguished from the atomic-like three-step model as found in a pioneering solid HHG study in monolayer h-BN [33], the physical insights of the novel four-step model would pave the way to realize the desktop solid-state soft X-ray light source. Last but not the least, we note that the essential features of HHG in the second plateau are not sensitive to the stacking pattern (see Fig. s3) and the type (see Fig. s4) of bilayer materials. We expect that the electron backscattering assisted HHG from distant bilayer would be optimized in multilayer array and even more complicated infrastructures, which could be fabricated by diverse nanoengineering technologies for practical application.

ACKNOWLEDGEMENTS

This work was supported by NSF of China Grant (No. 11704187, 11974185, 11774175 and 11834004), the Natural Science Foundation of Jiangsu Province (Grant No. BK20170032), Fundamental Research Funds for the Central Universities (No. 30920021153) and the Project funded by China Postdoctoral Science Foundation (Grant No.2019M661841). The Octopus code is available from www.octopus-code.org.

REFERENCES:

- [1] M. Hentschel, R. Kienberger, C. Spielmann, G. A. Reider, N. Milosevic, T. Brabec, P. Corkum, U. Heinzmann, M. Drescher and F. Krausz, *Nature* **414** 509 (2001).
- [2] P. Tzallas, D. Charalambidis, N. A. Papadogiannis, K. Witte and G. D. Tsakiris, *Nature* **426** 267 (2003).
- [3] G. Sansone, E. Benedetti, F. Calegari, C. Vozzi, L. Avaldi, R. Flammini, L. Poletto, P. Villoresi, C. Altucci, R. Velotta, S. Stagira, S. D. Silvestri and M. Nisoli, *Science* **314** 443 (2006).
- [4] E. Goulielmakis, M. Schultze, M. Hofstetter, V. S. Yakovlev, J. Gagnon, M. Uiberacker, A. L. Aquila, E. M. Gullikson, D. T. Attwood, R. Kienberger, F. Krausz and U. Kleineberg, *Science* **320** 1614 (2008).
- [5] F. Krausz and M. Ivanov, *Rev. Mod. Phys.* **81**, 163 (2009).
- [6] C. Winterfeldt, C. Spielmann, G. Gerber, *Rev. Mod. Phys.* **80**, 117(2008).
- [7] S. Ghimire *et al.*, *Nat. Phys.* **7**, 138 (2011).
- [8] O. Schubert *et al.*, *Nat. Photonics* **8**, 119 (2014).
- [9] G. Vampa, T. J. Hammond, N. Thiré B. E. Schmidt, F. Légaré C. R. McDonald, T. Brabec, and P. B. Corkum, *Nature (London)* **522**, 462 (2015).
- [10] M. Hohenleutner, F. Langer, O. Schubert, M. Knorr, U. Huttner, S.W. Koch, M. Kira, and R. Huber, *Nature (London)* **523**, 572 (2015).
- [11] T. T. Luu, M. Garg, S. Yu. Kruchinin, A. Moulet, M. Th. Hassan, and E. Goulielmakis, *Nature (London)* **521**, 498 (2015).
- [12] G. Ndabashimiye, S. Ghimire, M. Wu, D. A. Browne, K. J. Schafer, M. B. Gaarde, and D. A. Reis, *Nature (London)* **534**, 520 (2016).

- [13] N. Yoshikawa, T. Tamaya, K. Tanaka, *Science* **356**, 736 (2017)
- [14] S. Y. Kruchinin, F. Krausz, V. S. Yakovlev, *Rev. Mod. Phys.* **90**, 021002 (2018).
- [15] U. Huttner, M. Kira, and S.W. Koch, *Laser Photonics Rev.* **11**, 1700049 (2017).
- [16] S. Ghimire and D. A. Reis, *Nat. Phys.* **15**, 10 (2019).
- [17] C. Yu, S. Jiang, and R. Lu, *Advances in Physics: X* **4**, 1562982 (2019).
- [18] M. Garg, M. Zhan, T. T. Luu, H. Lakhotia, T. Klostermann, A. Guggenmos, and E. Goulielmakis, *Nature (London)* **538**, 359 (2016).
- [19] H. Kim, S. Han, Y. W. Kim, S. Kim, and S. W. Kim, *ACS Photonics* **4**, 1627 (2017)
- [20] M. Garg, H. Y. Kim, and E. Goulielmakis, *Nat. Photonics* **12**, 291 (2018).
- [21] F. Langer, M. Hohenleutner, C. P. Schmid, C. Poellmann, P. Nagler, T. Korn, C. Schüller, M. S. Sherwin, U. Huttner, J. T. Steiner, S. W. Koch, M. Kira, and R. Huber, *Nature (London)* **533**, 225 (2016).
- [22] R. E. F. Silva, Igor V. Blinov, Alexey N. Rubtsov, O. Smirnova, and M. Ivanov, *Nat. Photonics* **12**, 266 (2018).
- [23] S. A. Sørngård, S. I. Simonsen, J. P. Hansen, *Phys. Rev. A* **87**, 053803 (2013).
- [24] L. A. Chizhova, F. Libisch, J. Burgdörfer, *Phys. Rev. B* **95**, 085436 (2017)
- [25] J. D. Cox, A. Marini, and F. J. G. Abajo, *Nat. Commun.* **8**, 14380 (2017).
- [26] H. Liu, Y. Li, Y. S. You, S. Ghimire, T. F. Heinz, D. A. Reis, *Nat. Phys.* **13**, 262 (2017).
- [27] N. Tancogne-Dejean, O. D. Mücke, F. X. Kärtner, A. Rubio, *Phys. Rev. Lett.* **118**, 087403 (2017).
- [28] D. Dimitrovski, T. G. Pedersen, and L. B. Madsen, *Phys. Rev. A* **95**, 063420 (2017).
- [29] C. Yu, S. Jiang, T. Wu, G. Yuan, Z. Wang, C. Jin, and R. Lu, *Phys. Rev. B* **98**, 085439 (2018).
- [30] G. Vampa, C. R. McDonald, G. Orlando, D. D. Klug, P. B. Corkum, and T. Brabec, *Phys. Rev. Lett.* **113**, 073901 (2014)
- [31] G. Vampa, T. J. Hammond, N. Thiré B. E. Schmidt, F. Légaré C. R. McDonald, T. Brabec, D. D. Klug, and P. B. Corkum, *Phys. Rev. Lett.* **115**, 193603 (2015).
- [32] M. Wu, S. Ghimire, D. A. Reis, K. J. Schafer, and M. B. Gaarde, *Phys. Rev. A* **91**, 043839 (2015).
- [33] N. Tancogne-Dejean, and A. Rubio, *Sci. Adv.* **4**, eaao5207 (2018).
- [34] G. L. Breton, A. Rubio, and N. Tancogne-Dejean, *Phys. Rev. B* **98**, 165308 (2018).
- [35] H. Liu, C. Guo, G. Vampa, J. L. Zhang, T. Sarmiento, M. Xiao, P. H. Bucksbaum, J. Vučković, S. Fan, and D. A. Reis, *Nat. Phys.* **14**, 1006 (2018).
- [36] X. Andrade, D. Strubbe, U. De Giovannini, A. H. Larsen, M. J. Oliveira, J. Alberdi-Rodriguez, A. Varas, I. Theophilou, N. Helbig, M. J. Verstraete, L. Stella, F. Nogueira, A. Aspuru-Guzik, A. Castro, M. A. Marques, A. Rubio, *Phys. Chem. Chem. Phys.* **17**, 31371 (2015).
- [37] N. Tancogne-Dejean, O. D. Mücke, F. X. Kärtner, A. Rubio, *Nat. Commun.* **8**, 745 (2017).
- [38] N. Klemke, N. Tancogne-Dejean, G. M. Rossi, Y. Yang, F. Scheiba, R.E. Mainz, G. Di Sciacca, A. Rubio, F.X. Kärtner, and O. D. Mücke, *Nat. Commun.* **10**, 1319 (2019).
- [39] N. Tancogne-Dejean, M. A. Sentefand, and A. Rubio, *Phys. Rev. Lett.* **121**, 097402 (2018).
- [40] M. S. Mrudul, N. Tancogne-Dejean, A. Rubio, and G. Dixit, *npj Comput. Mater.* **6**,10 (2020).
- [41] K. J. Schafer, B. Yang, L. F. DiMauro, and K. C. Kulander, *Phys. Rev. Lett.* **70**, 1599 (1993).
- [42] P. B. Corkum, *Phys. Rev. Lett.* **71**, 1994 (1993).
- [43] C. I. Blaga, J. L. Xu, A. D. DiChiara, E. Sistrunk, K. Zhang, T. Miller, P. Agostini and L. F. DiMauro, and C. D. Lin, *Nature* **483**, 194 (2012).
- [44] M. Lewenstein, Ph. Balcou, M. Yu. Ivanov, A. L'Huillier, P. B. Corkum, *Phys. Rev. A* **49**, 2117 (1994).

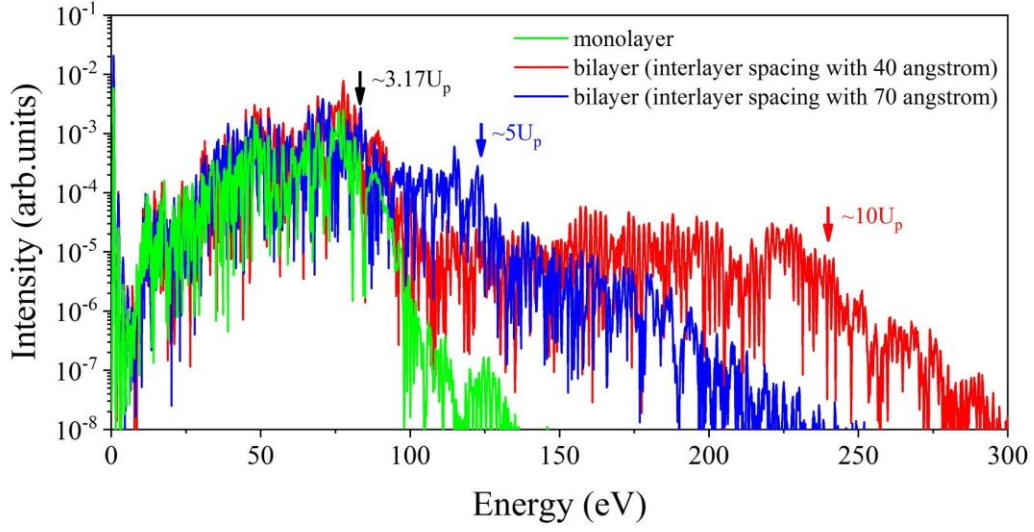


Fig. 1. High harmonic spectra from monolayer (green line), bilayer h-BN with interlayer spacing $d = 40$ angstrom (blue line) and $d = 70$ angstrom (red line).

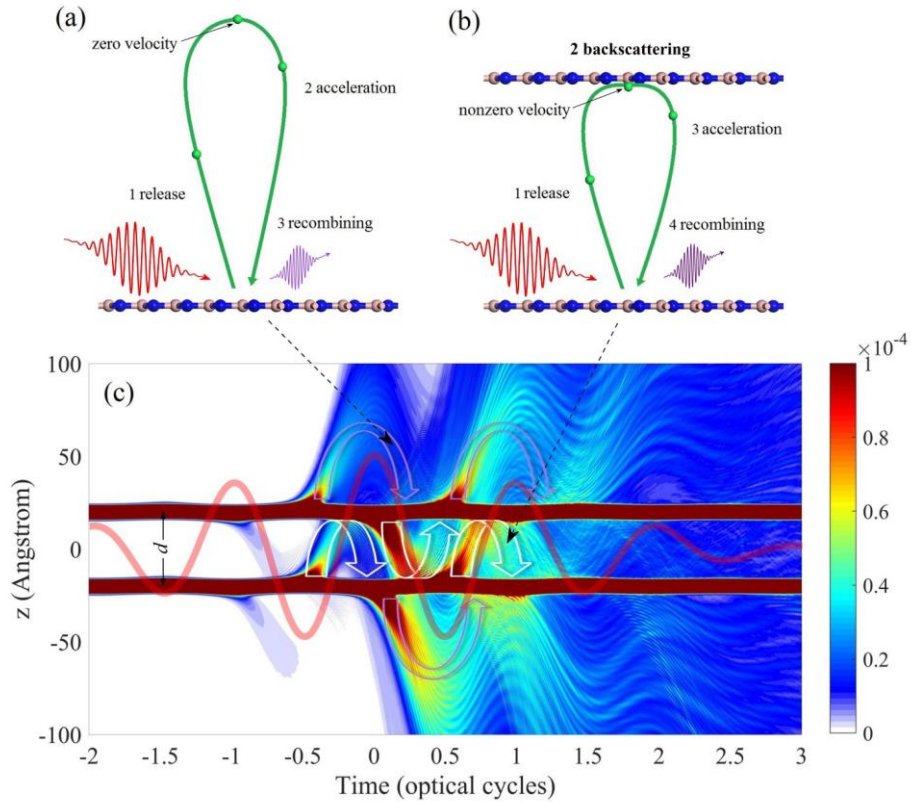


Fig. 2. Schematic HHG processes from (a) the traditional three-step model in monolayer h-BN and (b) the four-step model in distant bilayer h-BN. (c) Time evolution of the induced electronic density for distant bilayer h-BN. The interlayer spacing is $d = 40$ angstrom and laser parameters are the same as those in Fig. 1.

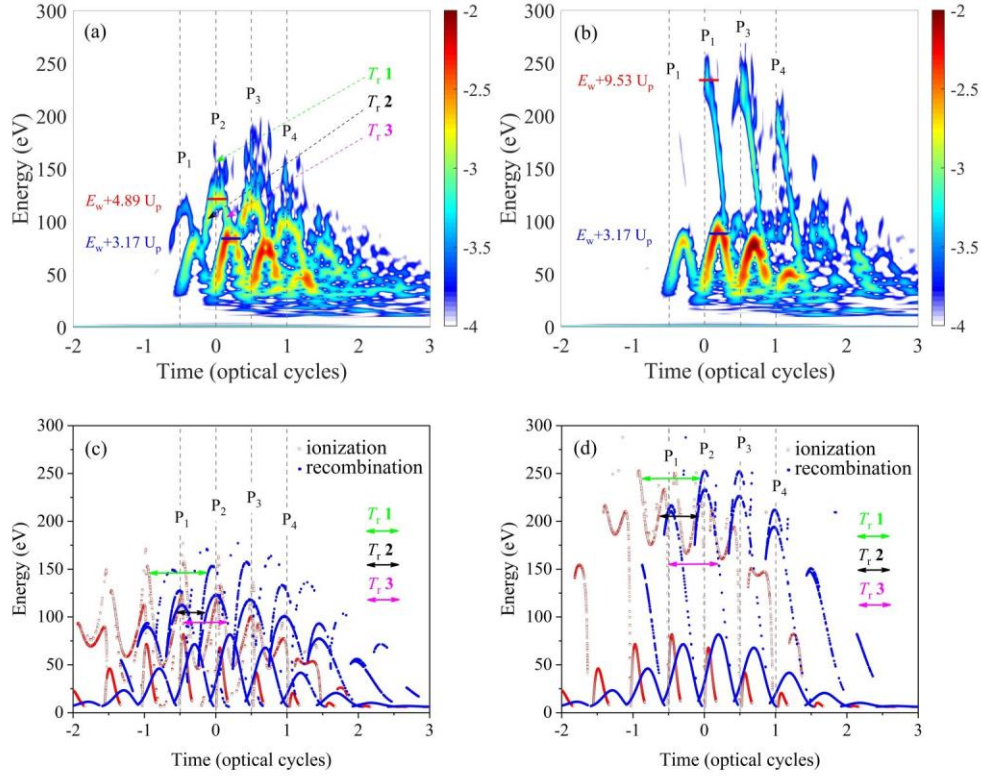


Fig. 3. Time-frequency analyses of HHG from distant bilayer h-BN for (a) $d = 40$ angstrom and (b) $d = 70$ angstrom. The classical ionization and recollision energy diagrams for distant bilayer h-BN with interlayer spacing of (c) $d = 40$ angstrom and (d) $d = 70$ angstrom.

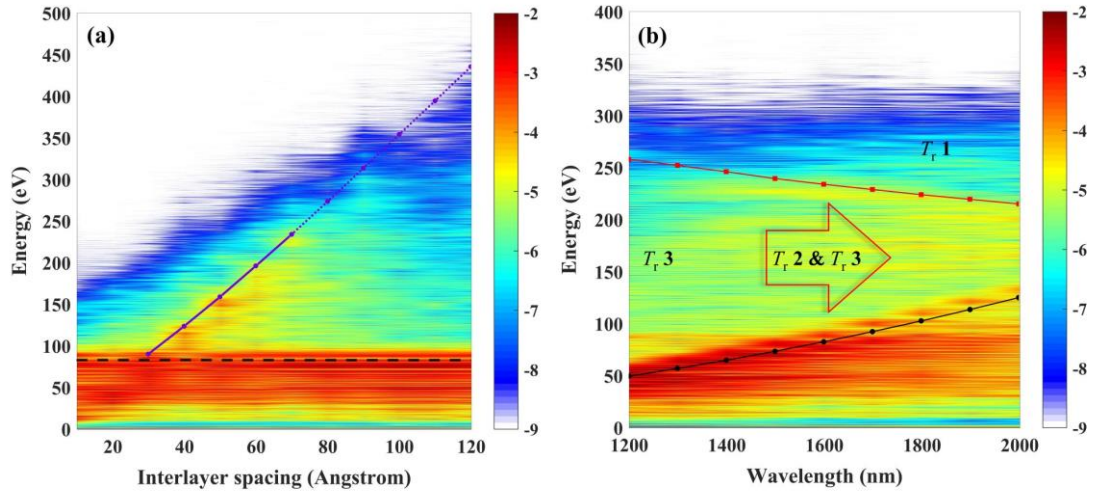


Fig. 4. (a) Interlayer spacing dependent HHG. The purple line represents the harmonic cutoff calculated by the classical model. The black dash line represents the cutoff in the first plateau. (b) The wavelength dependent HHG with fixed interlayer spacing $d = 70$ angstrom. The black line represents the cutoff in the first plateau and the red line represents the cutoff of trajectory **3** ($T_r 3$) in the second plateau.